Electrochimica Acta 528 (2025) 146188

Contents lists available at ScienceDirect

Electrochimica Acta

journal homepage: www.journals.elsevier.com/electrochimica-acta

A smart "Swiss-knife" dithiaaza[7]helicene electroactive tool: adding 3D push-pull features to inherent chirality and film electrodeposition ability

Luigi Menduti [a,§], Stefano Magni [a], Clara Baldoli [b], Silvia Rosa Araneo [a], Simona Rizzo [b], Benedetta Bertolotti [f], Alberto Bossi [b], Marta Penconi [b], Francesco Orsini [c], Francesca Romana Mammone [d], Claudio Villani [e], Francesca Fontana [f,g], Emanuela Licandro [a,b], Patrizia Romana Mussini [a,*]

[a] Università degli Studi di Milano, Dipartimento di Chimica, Via Golgi 19, 20133, Milano, Italy
[b] CNR-Istituto di Scienze e Tecnologie Chimiche (SCITEC) "Giulio Natta", Via C. Golgi 19, 20133 Milano and Via Fantoli 16/15, 20138, Milano, Italy
[c] Università degli Studi di Milano, Dipartimento di Fisica "Aldo Pontremoli", Via Celoria 16, 20133, Milano, Italy
[d] Centro Nazionale per il Controllo e la Valutazione dei Farmaci, Istituto Superiore di Sanità, Viale Regina Elena 299, 00161, Roma, Italy
[e] Università di Roma La Sapienza, Dipartimento di Scienza e Tecnologia del Farmaco, Piazzale Aldo Moro 5, 00185, Roma, Italy
[f] Università degli Studi di Bergamo, Dipartimento di Ingegneria e Scienze Applicate, Viale Marconi 5, 24044, Dalmine, (Bergamo), Italy
[g] CSGI Bergamo R.U., Viale Marconi 5, 24044 Dalmine, Italy

ARTICLE INFO

Keywords:
(Hetero)helicene structure/reactivity relationships
(Hetero)helicene electrochemistry
Push-pull conjugated systems
Inherently chiral electroactive molecules
Inherently chiral film electrodeposition

ABSTRACT

A new dithiaaza[7]helicene of remarkably multifaceted nature and functional properties is introduced and studied by comparison with a pool of simpler thia- or azahelicenes and related model molecules. Its helical conjugated backbone endows it with interesting spectroscopic and electrochemical features as well as with powerful inherent chirality. In addition, the new molecule has terminals of opposite character which endow it with push-pull features (along the backbone and across 3D space) as well as with a remarkable pool of functional properties: (*i*) an electron poor pyridine-based terminal, which can be involved in acid/base equilibria or enable conversion into molecular salts by alkylation; and (*ii*) an electron rich (benzodi)thiophene-based terminal, which allows reproducible electrodeposition of electroactive films, thus enabling to transfer the above pool of properties from single molecule to nanostructured inherently chiral electroactive materials.

1. Introduction

Helicenes are a class of polycyclic aromatic compounds made of ortho-fused benzene or other (hetero)aromatic rings, with a nonplanar screw-shaped skeleton [1–3]. When the number of rings is higher than five, they adopt a chiral helically-shaped conformation due to steric crowding between the two terminal rings of the molecule [4]; in this case the molecule can exist in two stable enantiomers that can be separated for instance by chiral HPLC [5]. The helical backbone is also a conjugated π-electron system highly delocalized not only along the condensed ring chain, but also across it, from π-stacking effects between rings overlapping in space [6]. Thus, in helicenes the whole molecular backbone is the source of both chirality and key functional properties (in particular, electronic ones), making them an outstanding example of powerful inherent chirality [7].

Such property can be propagated from the single molecule level to inherently chiral oligomer films, which can be conveniently prepared by electrodeposition from monomers with suitable electroactive terminals, obtaining enantiopure films with the same configuration of the starting monomer and enhanced effective conjugation [7–10].

Inherent chirality can afford impressive manifestations employing helicenes or helicene oligomer films as chiral selectors *e.g.* in chiral spectroscopy, chiral electrochemistry, and molecular spintronics [7, 11–15], three advanced fields in fascinating reciprocal interconnections still to be completely unveiled and exploited [16].

The presence of heteroatom(s) in the helical backbone (resulting in *hetero*helicenes) enables to significantly modulate helicene properties respect to carbohelicene cases, affecting *e.g.* geometric parameters, electronic properties, redox site localization, conjugation efficiency, molecular interactions, and oligomerization ability; this prompted many

* Corresponding author.
E-mail address: patrizia.mussini@unimi.it (P.R. Mussini).
§ Current address: Università degli Studi di Milano, Dipartimento di Scienze Farmaceutiche, Via Mangiagalli 25, 20133 Milano.

https://doi.org/10.1016/j.electacta.2025.146188
Received 14 February 2025; Received in revised form 1 April 2025; Accepted 2 April 2025
Available online 6 April 2025

research groups to focus on heterohelicenes and heterohelicenoids [2,3,7,8,17–22].

Heterohelicenes can entirely consist of heteroaromatic rings, or, more commonly, consist of either a sequence of heteroaromatic rings regularly alternated with aromatic carbocylic ones, or a carbohelicene sequence featuring one or more randomly inserted heteroaromatic rings. The most popular heterohelicene families are:

- pyridine-based *aza*helicenes, electron poorer than carbohelicenes, and the properties of which can be modulated by acid-base equilibria (for example, symmetrically pyridine-terminated 1,14-diazahelicene has been recently reported as a superbase/proton sponge exploited as a matrix for matrix-assisted ionization/laser desorption MALDI spectroscopy for acid analytes [23]) and quaternarization, both properties being based on the N atoms, whose lone pairs are not involved in the overall conjugation. The latter feature affords inherently chiral molecular salts, which could possibly include inherently chiral ionic liquids, if the melting point could be sufficiently lowered by appropriate choice of alkyl substituent and counterion [18,19,24];
- thiophene-based *thia*helicenes, electron richer than carbohelicenes, and easier to (electro)oligomerize into inherently chiral electroactive films with attractive functional properties for smart chiral devices in organic electronics and spintronics [7,8].

Heterohelicenes are usually based on a single kind of heteroaromatic ring, as in the above main two classes; however, quite attractive is the development of helicenes incorporating different heteroaromatic rings, resulting in multifunctional inherently chiral tools, endowed with the properties of both heteroaromatic rings. Very few examples of thiaazahelicenes or smaller analogues have been reported in the literature so far [25]. Particularly interesting is the case in which each helicene terminal coincides with a different heteroaromatic ring, possibly resulting in "push-pull" electronic effects both along the helical chain and vertically in 3D space between the partially or totally superimposed terminals.

In this frame, the dithiaaza[7]helicene **1** (Chart 1) has been prepared and investigated by both spectroscopic and electrochemical methods, particularly focusing on its electronic properties and film electrodeposition ability.

To better interpret the results, the study also involves a systematic series of models including:

- the alkene precursor **2** of dithiaaza[7]helicene **1**, to evaluate modification of electronic properties upon conversion into the helical structure implying a torsional angle as well as possible π-stacking effects;
- the dithia[7]helicene **3**, analogue of **1** with a benzene terminal instead of the pyridine one, together with its alkene precursor **4**, as models for the benzodithiophene (BDT)-terminated side;
- the 7-ring and 6-ring azahelicene analogues of **1** without the BDT terminal, **5** and **6** respectively, as models for the pyridine-terminated side.

2. Results and discussion

2.1. Synthesis of helicenes *1, 3, 5* and *6* and related alkene precursors *2, 4, 7* and *8*

Helicenes **1**, **3, 5** and **6** (Chart 1) have been prepared using the classical Mallory photochemical reaction [26,27] which allows to build the helix, through the formation of an additional benzene ring, starting from the appropriate alkene precursors. As reported in Scheme 1 for the case of helicene **1**, the irradiation of solutions of alkenes **2, 4, 7** and **8** in ethyl acetate with a medium pressure Hg lamp (125 W) gave the corresponding helicenes **1, 3, 5** and **6**. The present work *inter alia* confirms that the Mallory photochemical route [25] is a versatile methodology to access to helical systems of which **1**, **3** and **5** are new compounds while aza[6]helicene **6** has already been reported [28].

The synthesis of alkene precursors **2, 4, 7** and **8** (Scheme 2) was performed through a Wittig reaction between aldehyde **9a-c** and the triphenylphosphonium salt **10a-c**, with DBU (alkenes **2** and **4**) or *t*-BuOK (alkenes **7** and **8**) as a base to generate the corresponding ylide. [See SI for experimental details and product characterization] All alkenes were obtained as mixture of *E/Z* isomers and used as such for the photocyclization reaction to prepare helicenes. Pure *E* isomers of alkenes **2** and **4**, were obtained from the purification of the isomeric mixture (see SI), and were used in photophysical and electrochemical studies.

2.2. HPLC enantioseparation of dithiaaza[7]helicene *1*

A preliminary chromatography study on a chiral stationary phase (CSP) has been carried out on the analytical resolution of the racemic dithiaaza[7]helicene **1** into its (*P*)- and (*M*)- enantiomers, a key feature for a quantum leap in future applications. The enantioseparation has been successfully achieved (Fig. 1) with a Chiralpak IA 5 μm column, at r.t., using *n*-hexane/CH_2Cl_2 60:40 (v/v) as the mobile phase.

Also in the case of 2-aza[7]helicene **5** a chiral HPLC study has been carried out, and the enantiomers successfully detected by circular dichroism CD (details in the SI).

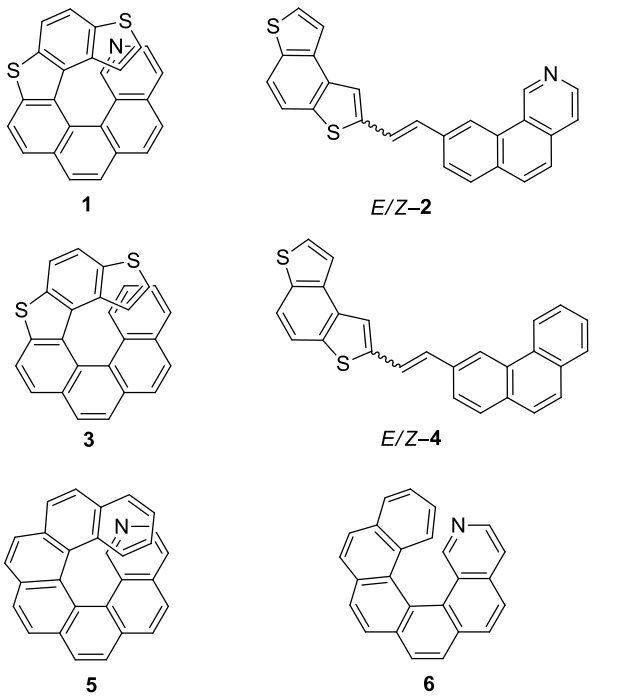

Chart 1. The investigated helical systems and related precursors.

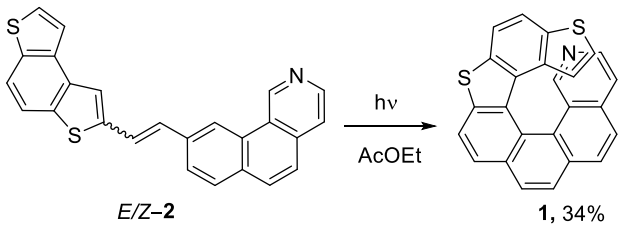

Scheme 1. Photocyclization of alkene **2** into helicene **1**.

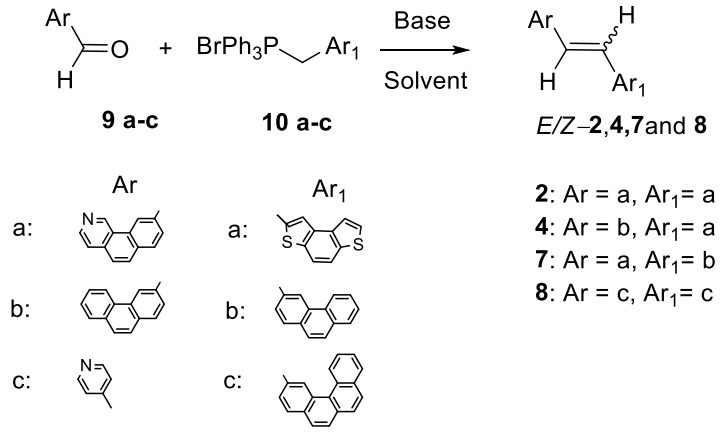

Scheme 2. Synthesis of alkene precursors **2, 4, 7** and **8**.

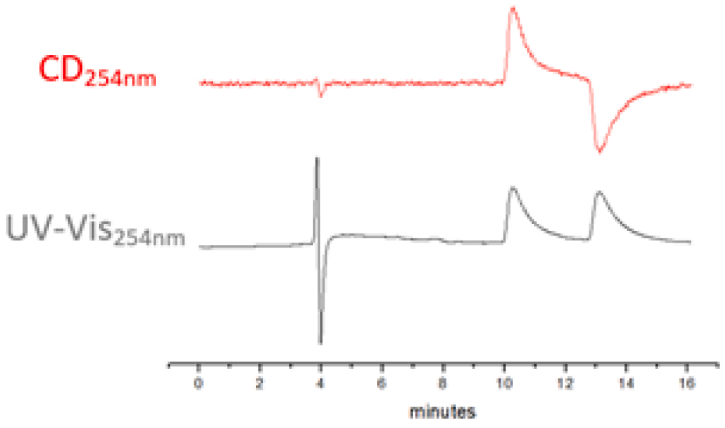

Fig. 1. HPLC enantioseparation of helicene **1** monitored by UV and CD detectors. Chromatographic conditions: column, Chiralpak IA (250 mm × 4.6 mm, 5 μm); mobile phase, *n*-hexane/CH_2Cl_2 60:40 (v/v); temperature, 25 °C; flow rate, 1.0 cm^3/min; detection, UV/CD at 254 nm.

2.3. *Investigation of electronic properties*

The electronic properties of the new dithiaaza[7]helicene **1** and some related model compounds were investigated both spectroscopically, in terms of UV–Vis absorption and emission properties, and electrochemically, by cyclic voltammetry CV and differential pulse voltammetry DPV.

2.3.1. *Optical UV-Vis absorption and emission features*

Fig. 2 and Figure S10 (with key data summarized in Table 1) show the UV–Vis absorption spectra of the new dithiaaza[7]helicene **1** and of its dithia[7]helicene analogue **3**, as well as of their *E*-alkene precursors **2** and **4**, for comparative purposes.

Both alkene precursors **2** and **4** display a structured absorption profile with four clearly resolved peaks between 330 and 430 nm (λ_{max} = 397 nm, ε_{max} = 3.7 × 104 cm^{-1} M^{-1} for alkene **2**) spaced by 1400–1500 cm^{-1}. Interestingly, the related pattern is nearly identical to that of benzodithiophene BDT, previously reported by some of us in similar conditions [8,29] although the peaks are redshifted by some 100 nm, which could of course be ascribed to the increased overall conjugation of the molecular π-system. Moreover, both shape and wavelength of such absorption bands are almost identical for *E*-**2** and *E*-**4** (*i.e.* regardless of the nature of the benzene/pyridine terminal ring), which would point to the first absorption process being mostly determined by the BDT moiety.

This assumption looks consistent with both azaphenanthrene and phenanthrene having unstructured absorption features located at shorter wavelengths than BDT; furthermore, also the tetrathiaalkene

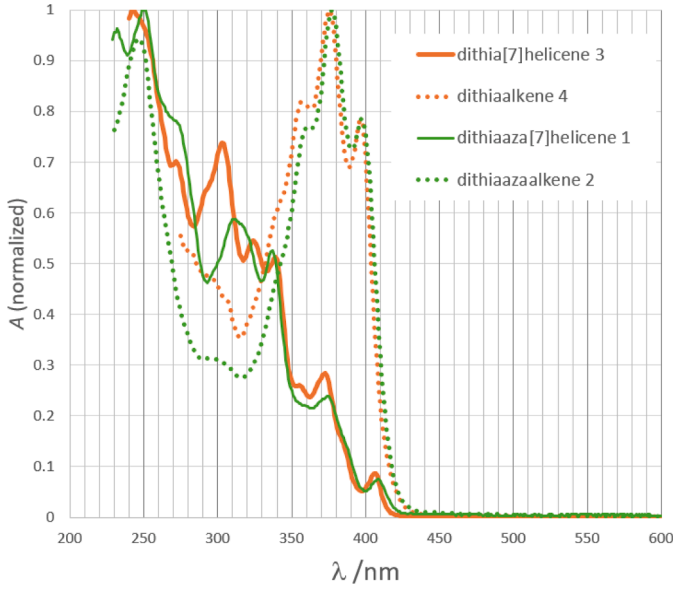

Fig. 2. A synopsis of UV–Vis absorption spectra (normalized *vs* the maximum absorbance peak) for helicene **1** (green solid line) with alkene precursor *E*-**2** (green dotted line) and helicene **3** (orange solid line) with alkene precursor *E*-**4** (orange dotted line), in CH_2Cl_2.

Table 1
A selection of key spectroscopic and electrochemical parameters of the new dithiaaza[7]helicene **1** compared with selected model compounds.

		$\lambda_{max(ons)abs}$ /nm	$E_{g\ max(ons)abs}$ /eV	$\lambda_{max\ em}$ /nm		$E_{p,c}$ *vs* Fc^+|Fc /V	$E_{p,a}$ *vs* Fc^+|Fc /V	$E_{g\ max,EC}$ /eV
"Carbo" model compounds								
Carbo[6]helicene **S16**	[9,10]				CH_3CN, TBAP	*~−2.4/−2.5*[a]	*~1.1/1.3*[a]	*~3.7*
Carbo[7]helicene **S17**	[9,10]				CH_3CN, TBAP	*~*−2.4/*−2.5*[a]	*~1.05/1.25*[a]	*~3.6*
"Thia" model compounds								
Benzodithiophene **BDT**	[8]	318 (324)	3.90 (3.83)		CH_2Cl_2, TBAP	−3.00	1.12	4.12
Tetrathia *E* alkene precursor **S10**	[29,32]	416 (~440)	2.98 (~2.82)	428 (0.75 ns, QY 0.41)	THF,$TBAPF_6$			2.7
(7,8-dipropyl)tetrathia *Z* alkene precursor **S11**	[29]	310,340[sh] (~410)	4.00,3.65[sh] (~3.03)					
Tetrathia[7]helicene **S9**	[8,29]	386 (407) 387 (~410)	3.46 (3.07) 3.21 (~3.03)	403 (0.74 ns, QY 0.06)	CH_2Cl_2, TBAP	−2.59	0.86	3.21
	[7]				CH_2Cl_2, $TBAPF_6$		0.92	
	[7]				CH_3CN, $TBAPF_6$	−2.47	0.88	3.35
(7,8-dipropyl)tetrathia[7]helicene **S12**	[29]	390 (~410)	3.18 (~3.03)	401 (0.88 ns, QY 0.10)	CH_2Cl_2, TBAP	−2.67	0.87	3.24
(7,8,13,14-tetrapropyl)hexathia[11]-helicene **S13**	[8]	440 (469)	3.14 (2.88)		CH_2Cl_2, TBAP	−2.49	0.65, 0.96	2.82
Dithiaalkene precursor **4**		398 (418)	3.12 (2.97)		CH_3CN, $TBAPF_6$	−3.00, −2.44,−2.28	0.78, 1.00	3.06
Dithia[7]helicene **3**		*405 (~420),* 388/375/303	3.07 (*~2.96)* 3.20/3.31/4.1		CH_3CN, $TBAPF_6$	−2.77, −2.65,−2.44	0.92	3.36
"Aza" model compounds								
5-aza[6]helicene **S14**	[18]				CH_3CN, $TBAPF_6$	−2.66,−2.52, −2.25	1.07, 1.47	3.32
2,12-diaza[6]helicene **S14**	[19]				CH_3CN, $TBAPF_6$	−2.73,−2.48, −2.41,−2.16	1.26	3.42
2-Aza[6]helicene **6**					CH_3CN, $TBAPF_6$	−2.86, −2.54,−2.34	(?), 1.37	*(?), 3.71*
2-Aza[7]helicene **5**					CH_3CN, $TBAPF_6$	−2.77,−2.58, −2.34	*0.98?*, 1.29	*3.32? 3.63*
"Thiaaza" compounds								
Dithiaazaalkene precursor **2**		397 (422)	3.13 (2.94)	440 (0.86 ns, QY 0.65)	CH_3CN, $TBAPF_6$	−3.01,−2.64, −2.39,−2.20	0.76,0.90, 1.06	2.96,3.10
Dithiaaza[7]helicene **1**		*408 (~425),* 380/338/305	*3.07 (~2.96)* 3.20/3.31/4.1	420 (0.52 ns, QY 0.015)	CH_3CN, $TBAPF_6$	−2.84,−2.67, −2.30	0.97, 1.18	3.27

Spectroscopy experiments have been performed in CH_2Cl_2. [a]Approximately estimated from voltammograms reported in papers [9] and [10], applying the potential normalization term reported by the authors. [Sh] = shoulder.

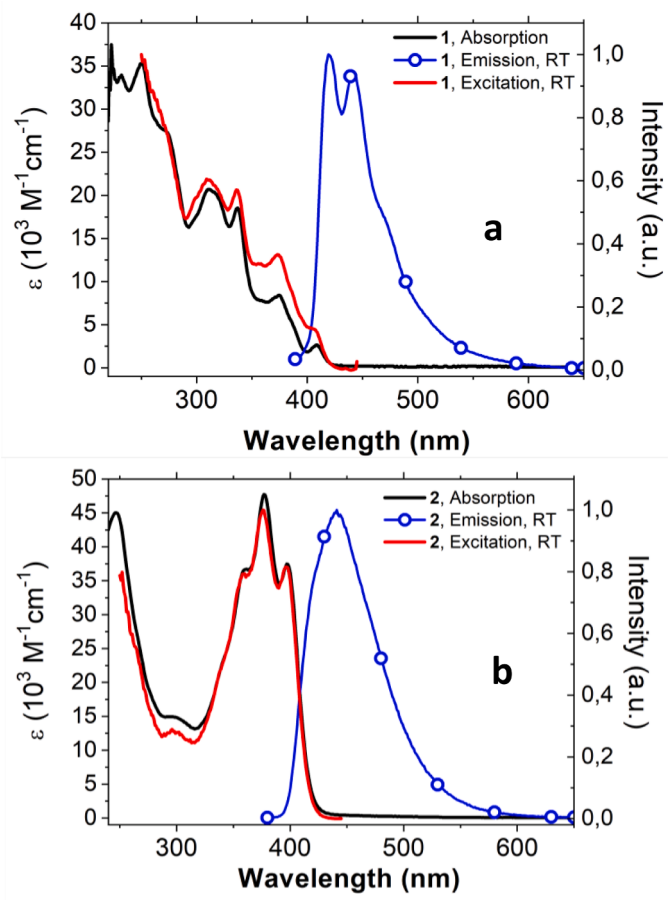

Fig. 3. Absorption (black), excitation (red) and emission (blue) spectra at room temperature, CH_2Cl_2: a) helicene **1**; b) alkene *E*-**2**.

precursor of tetrathia[7]helicene [8] has a absorption pattern similar to alkenes **2** and **4**, although more finely resolved and redshifted by about 20 nm ([29], Table 1). This would also indicate that the benzene rings contribute less effectively than thiophene ones to the overall conjugation at constant aromatic ring number.

Helicenes **1** and **3** share a nearly identical absorption pattern between 330 and 410 nm, with the lowest energy peak being located at 408 nm with absorptivity of only 2.6×10^3 $cm^{-1}M^{-1}$ for helicene **1**. This portion of the spectrum differs in shape from the "BDT pattern" described earlier and shows significantly lower intensity than the absorptivities of **2** and **4**. In contrast, the absorptions in the 270–330 nm region where alkenes **2** and **4** show low absorptivities are much more intense in helicenes **1** and **3** (and consistent with electrochemical HOMO-LUMO data for the same molecules, see Table 1 and next paragraph); moreover, they notably differ between helicenes **1** and **3**, likely accounting for their diverse chemical structures and different interactions between the thiophene terminal and the pyridine/benzene one.

Overall, the spectral patterns of helicenes **1** and **3** suggest a reduction in conjugation efficiency relative to their precursors **2** and **4**, which can be attributed to the torsional angle of the helix introduced by benzannulation.

Precursor dithiaazaalkene **2** in *E* configuration (Fig. 3b) displays an unstructured fluorescence band observed at $\lambda_{max} = 440$ nm, with lifetime = 0.86 ns and quantum yield = 65 %, in contrast to previous examples of symmetrically substituted alkenes ([29] and Table 1) featuring structured luminescence (as well as significantly smaller Stokes shifts). This might point not only to more conformational freedom degrees, but also to an excited state characterized by a slight charge transfer character, which would account for the donor-acceptor structure of the molecule.

Instead, a structured fluorescent emission is well perceivable in dithiaaza[7]helicene **1**, with $\lambda_{max} = 420$ nm, lifetime = 0.52 ns and quantum yield = 1.5 % (Fig. 3a). The blue shifted spectrum is indicative of a slightly reduced conjugation efficiency of the helical framework compared to precursor **2**, while the vibrationally resolved peak in **1** could account for the more rigid system. Concerning the observed quantum yields for **1** *vs* **2**, they can be considered in line with previous studies where helicenes are tipically less efficient emitters compared to the precursor alkenes (*e.g.* [29]). Alkenes have a quite rigid structure in the *E* configuration where excited states are as planar as the ground one; thus conjugation is particularly efficient across the *E* configuration of the double bond reducing potentially hampering deactivation pathways.

2.3.2. *Electrochemical properties*

An extensive cyclic voltammetry (CV) and differential pulse voltammetry (DPV) study (Table 1, Figs. 4 and 5, Figures S11-S36) was performed to highlight the electron transfer properties of

(i) the new dithiaaza[7]helicene **1**;
(ii) helicenes **3, 5** and **6**, as models featuring a single heteroaromatic terminal, either benzodithiophene (helicene **3**, with a helical backbone dimensionally nearly coincident with **1** having the same sequence of five and six-membered rings), or pyridine (**5** or **6**, with all-six-membered ring helical backbones, thus slightly larger and slightly shorter than **1**, respectively);
(iii) precursor alkenes **2** and **4**, to evaluate the effect of cyclization on the electron transfer properties.

The investigation was performed on glassy carbon GC working electrodes, in CH_3CN with 0.1 M $TBAPF_6$ as supporting electrolyte (details in the SI). It enabled us:

- to evaluate whether a given ET be chemically reversible (*i.e.* leads to a stable product with no subsequent chemical steps in the chosen timescale) from the presence of a reversible return peak;
- to evaluate whether a given ET be electrochemically reversible, *i.e.* kinetically facile, accounted for by constant peak potential with increasing scan rate;
- in the case of a chemically irreversible ET, to highlight the possible formation of filming electroactive products or oligo/polymer films on the electrode surface, and to study their features;
- to experimentally evaluate HOMO and LUMO energies (from first oxidation and first reduction potentials, respectively, see SI) as well as HOMO-LUMO gaps to be compared with spectroscopic ones. It is useful to remark that the two approaches are expected to yield consistent results (although not coincident, since electrochemistry implies the presence of net charges and of a supporting electrolyte) provided that, as in most cases, the HOMO and LUMO orbitals involved in the electron transition coincide with those corresponding to first oxidation and first reduction. Actually, dealing with thermodynamic quantities, implying minimization of kinetic contributions, reliable HOMO and LUMO evaluation from electrochemical data applies to kinetically facile (electrochemically reversible, or at least quasi reversible) electron transfer processes only; luckily, many highly conjugated systems comply with such condition (see scan rate studies for our systems in the SI);
- by comparison of the above features in systematic series, to deduce rationalizing guidelines for the family.

As a background for discussing the voltammetry features of the present new compounds, it is useful to recall some observations from previous studies concerning a pool of related molecules, of which key data are also reported in Table 1 for the sake of comparison (when needed after proper normalization of the reported potentials *vs* the

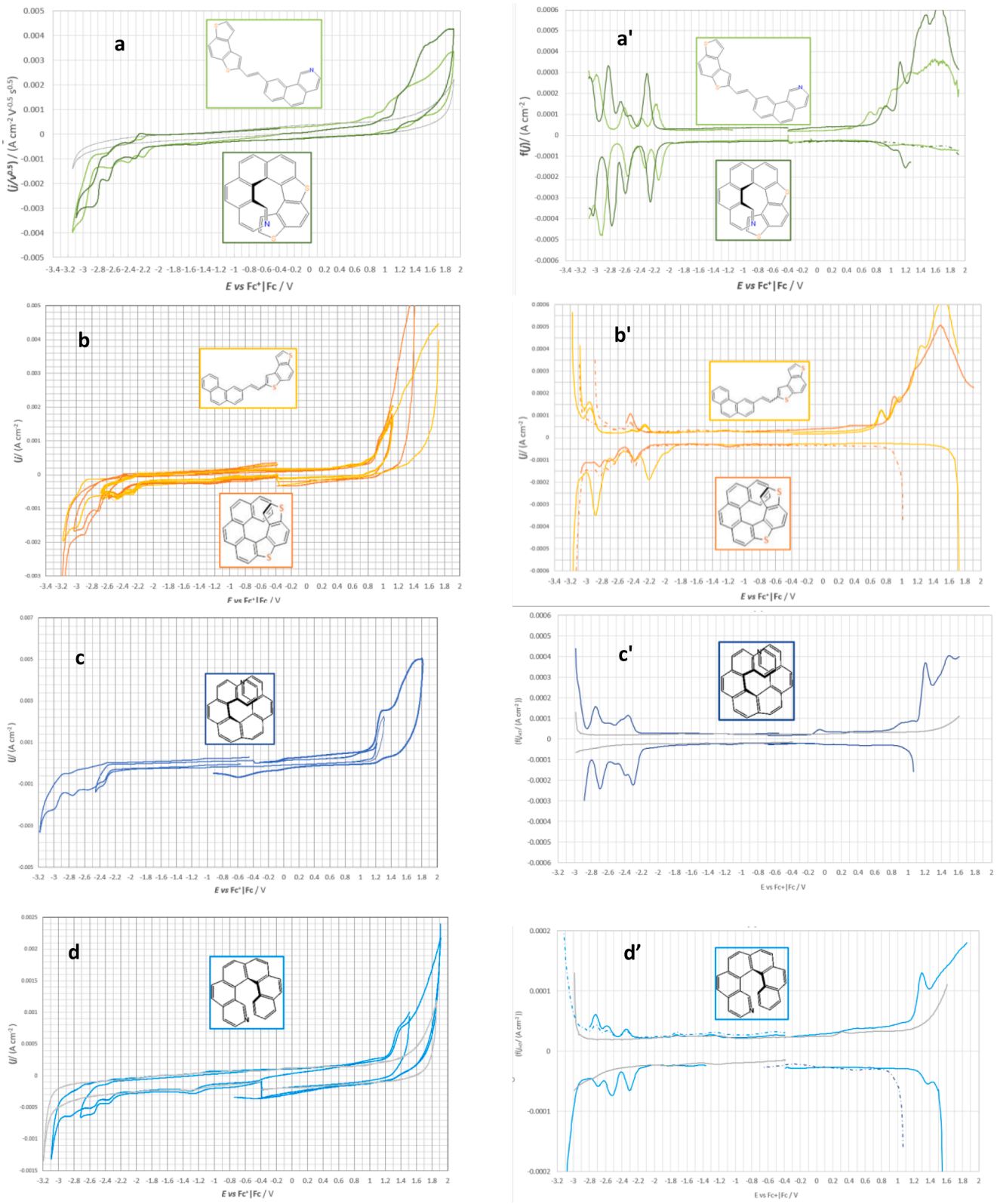

Fig. 4. CV (left) and DPV (right) features, recorded on GC in CH_3CN + 0.1 M $TBAPF_6$ at 0.2 V/s, of (from top to bottom): dithiaaza[7]helicene **1** *vs* dithiaazaalkene precursor **2**; dithia[7]helicene **3** *vs* dithiaalkene precursor **4**; 2-aza[7]helicene **5**; 2-aza[6]helicene **6**.

intersolvental reference redox couple ferrocene [30]; also in the following discussion all mentioned potentials are reported *vs* $Fc^+|Fc$).

For the benzodithiophene BDT (Chart S1) building block, investigated in similar conditions as the present ones except for the slightly different supporting electrolyte (TBAP instead of $TBAPF_6$), a single reduction peak and a single oxidation peak, both of them looking chemically irreversible, were observed in the potential window, at $E_{p,Ic} = -3.00$ V and at $E_{p,Ia} = +1.12$ V [8], resulting in a 4.1 eV HOMO-LUMO gap, consistent with the reported spectroscopic 3.9 eV one.

In the same conditions, tetrathia[7]helicene (**S9** in Chart S1),

consisting of four thiophenes (T) alternated with three benzenes (B) in a TBTBTBT sequence, which could also be regarded as two BDT units joined by a benzene ring, showed a sequence of electron transfers on both the oxidation and the reduction side, starting at much milder potentials, consistently with the much higher overall conjugation. In particular, the first reduction peak, possibly chemically (quasi) reversible, is located at $E_{p,Ic} = -2.47$ V, while the first oxidation one, located at $E_{p,Ia} = +0.88$ V, is chemically irreversible and results in electrodeposition of an electroactive film including coupling products, particularly dimers [7]. The HOMO-LUMO gap, 3.4 eV, is intermediate between those of linear α-terthiophene and α-tetrathiophene [31], which is reasonable considering that the overall conjugation of tetrathiahelicene is mainly contributed by the four conjugated thiophenes, which however do not reach the efficiency of linear α-tetrathiophene due to the loss of planarity from the system torsion.

The symmetrical *E* alkene precursor of tetrathia[7]helicene (**S10** in Chart S1), analogous to **2** and **4** but with both BDT terminals, has been also described [29,32] providing unfortunately only very partial and hardly normalizable electrochemical data (in THF + 0.1 M $TBAPF_6$); however, a comparison of HOMO-LUMO gaps, both spectroscopic and electrochemical (Table 1), highlights the remarkable decrease in conjugation efficiency in the helical compound respect to the linear alkene precursor.

Interestingly, in the same paper [29] a dramatically different UV–Vis spectrum is shown by the same alkene precursor in *Z* configuration (**S11** in Chart S1; it actually features two additional propyl chains in 7,8 positions respect to the *E* stereoisomer, but their effect is nearly negligible in this context, as confirmed by the corresponding non-alkylated and alkylated helicenes, **S9** and **S12** in Chart S1, having practically the same UV–Vis features and only slightly different CV ones). The first absorption band of the **S11** *Z* isomer is much less defined and with a remarkably blue shifted maximum (310 nm *vs* 416 nm, Table 1) respect to the **S10** *E* isomer, and the HOMO-LUMO gap is dramatically larger (4 eV *vs* 2.98 eV), pointing to a much lower conjugation efficiency, possibly on account of a less efficient orbital combination. Remarkably, the **S11** absorption maximum is blue shifted and its HOMO-LUMO gap larger also respect to the corresponding helicene **S12**, on account of the central benzene ring in **S12** forcing the two BDT subunits in a reciprocal position more favourable for conjugation [29].

Longer hexathia[11]helicene TBTBTBTBTBT (tetraalkylated in 7,8,13,14 positions, **S13** in Chart S1, Table 1) showed even milder first oxidation and reduction potentials and a smaller gap [8]. Interestingly, in this case the first oxidation corresponds to a chemically reversible twin peak system resulting in no oligomerization. This is consistent with the extensive superimposition of the molecule terminals, which possibly behave as equivalent interacting redox centres, and also with the presence of four long alkyl chains.

In the case of azahelicenes the interpretation of oxidation processes is more complex and direct comparison with other helicenes more difficult, since oxidation of the N lone pair, which is not directly involved in the aromatic system, should be taken into account as a possible process, too, besides radical cation formation on the aromatic system. In this respect, also the N position respect to the closest benzene ring could matter, the α, quinoline-like one resulting in more interactions between the N lone pair and the aromatic system with respect to the β, isoquinoline-like one (for example, for this reason quinoline is significantly less basic than isoquinoline). Former studies report electrochemical data for 5-aza-[6]helicene [18] (**S14** in Chart S1), which features a BPBBBB sequence of one pyridine and five benzene rings in which the nitrogen atom is in quinoline-like position and pointing externally, *i.e.* is sterically unhindered, and for 2,12-diaza[6]helicene [19] (**S15** in Chart S1), featuring a PBBBPB sequence of four benzene and two pyridine rings, in which one nitrogen atom is in the same unhindered, quinoline-like position, while the other one is in isoquinoline-like position; interestingly, in spite of being in a strongly hindered position the latter is the first one to undergo oxidative alkylation [19]. Both azahelicenes have their first reduction peaks at potentials significantly less negative than tetrathiahelicene, consistently with their electron poorer character and increasingly with the number of pyridine rings ($E_{p,Ic} = -2.25$ V for the monoaza and $E_{p,Ic} = -2.16$ V for the diaza case, followed by a sequence of further reduction steps). Instead the reported first oxidation peaks are located at $E_{p,Ia} = +1.07$ V for the monoaza and at $E_{p,Ia} = +1.26$ V for the diaza (where first oxidation concerns the isoquinoline-like N atom in 2-position), an intriguing difference looking only partially consistent with inductive effects.

Two papers [9,10] are also available concerning the electrochemistry of carbohelicenes consisting of 6 or 7 condensed benzene rings, *i.e.* slightly longer/shorter than the dithiaazahelicene backbone (**S16** and **S17** in Chart S1), although mostly focusing on the electrodeposition and characterization of electroactive films. From reported CV figures the first oxidation step looks in both cases irreversible and resulting in electrodeposition of an electroactive film, while the first reduction looks reversible/quasi reversible and possibly monoelectronic. From the same figures (and applying the reported potential normalization term), both carbo[7]- **S17** and carbo[6]helicene **S16** feature, respect to tetrathia[7]helicene **S9**, a much more positive first oxidation peak potential together with a similar first reduction peak potential. This could be explained in terms of a negative potential shift for both oxidation and reduction processes originating from the electron richer character of tetrathia[7]helicene **S9**, combined with the narrowing of the gap between first oxidation and first reduction originating from the tetrathia[7]helicene more effective global conjugation. Overall, the carbohelicene first reduction potentials look significantly more negative than the azahelicene ones, consistently with the electron poorer nature of the latter, while first oxidations are closer to the azahelicene ones (which however could concern N oxidation) or slightly more positive. As a consequence, the carbohelicenes have significantly larger HOMO-LUMO gaps than both the above discussed thia- or azahelicenes.

With this background we can now focus the discussion on the new compounds.

The dithiaazaalkene precursor **2** has (Table 1, Fig. 4a and a') on the reduction side a sequence of three very regular peaks, reversible both electrochemically and chemically (Figure S13), the first one of which being located at $E_{p,Ic} = -2.20$ V, before a fourth less canonical signal close to the background. Therefore, the highly conjugated system can support three subsequent electron uptakes at close potentials, kinetically facile and resulting in stable forms of the molecule. Also on the oxidation side a sequence of peaks can be observed, but much less well defined, with lower currents and only weak hints of chemical reversibility (although the first ET appears fast on account of the oxidation potential nearly constant with scan rate), with $E_{p,Ia} = +0.76$ V.

By comparison (graphically available in Figure S35), the dithiaalkene precursor **4** (Table 1, Fig. 4b, b', S15) features a slightly more positive first oxidation peak ($E_{p,Ia} = +0.78$ V) while the first reduction step is negatively shifted by nearly 0.1 V ($E_{p,Ic} = -2.28$ V); the resulting electrochemical HOMO-LUMO gaps are 2.96 eV for **2** and 3.06 eV for **4**. Such differences could be explained considering that the first reduction step should be mostly localized on the electron poorer benzoquinoline terminal, while the attracting inductive effects of the latter [33] would be negligible for the far away BDT terminal on which the first oxidation should be localized. In turn, comparing the three spectroscopic HOMO-LUMO gaps of **S10, 4** and **2** in Table 1, the overall conjugation efficiency of both **2** and **4** is lower than that of the symmetrical tetrathiaalkene **S10** precursor of tetrathiahelicene **S9**, highlighting the more effective contribution to the overall conjugation of thiophene units respect to benzene ones.

Dithiaaza[7]helicene **1** has CV and DPV characteristics quite similar to its precursor **2** (Table 1, Fig. 4a, a', S11, S12) but with lower peak multiplicity on both sides, and with potentials shifted towards more extreme values for both first oxidations and first reductions, with $E_{p,Ic} = -2.30$ V and $E_{p,Ia} = +0.97$ V; the HOMO-LUMO gap is therefore 3.27 eV,

significantly narrower than that of the alkene precursor. These observations clearly account for the loss of planarity of the system, resulting in significantly lower conjugation efficiency. As already mentioned, when moving from precursor to the helicene, it seems, especially looking at the DPV but also carefully looking at the CV, that a single signal takes the place of a previous pair of signals, both on the oxidation side and on the reduction side. In fact, if the terminals were significantly overlapped (with interaction in π stacking prevailing compared to that through the planar conjugated system of the precursor) and therefore no longer independent, they could be involved simultaneously in single oxidation and reduction processes; and the way of hosting the charges that form along the conjugated system could also change significantly.

Similar remarks can be made also for dithia[7]helicene **3** ($E_{p,Ic}$ = −2.44 V, $E_{p,Ia}$ = +0.92 V; E_{gap} = 3.36 eV, (Table 1, Fig. 4b, b', S14) respect to its precursor **4**; and, notably, in the two available helicene *vs* precursor couples (**1** *vs* **2**, **3** *vs* **4**) the E_{gap} increase upon helicization is

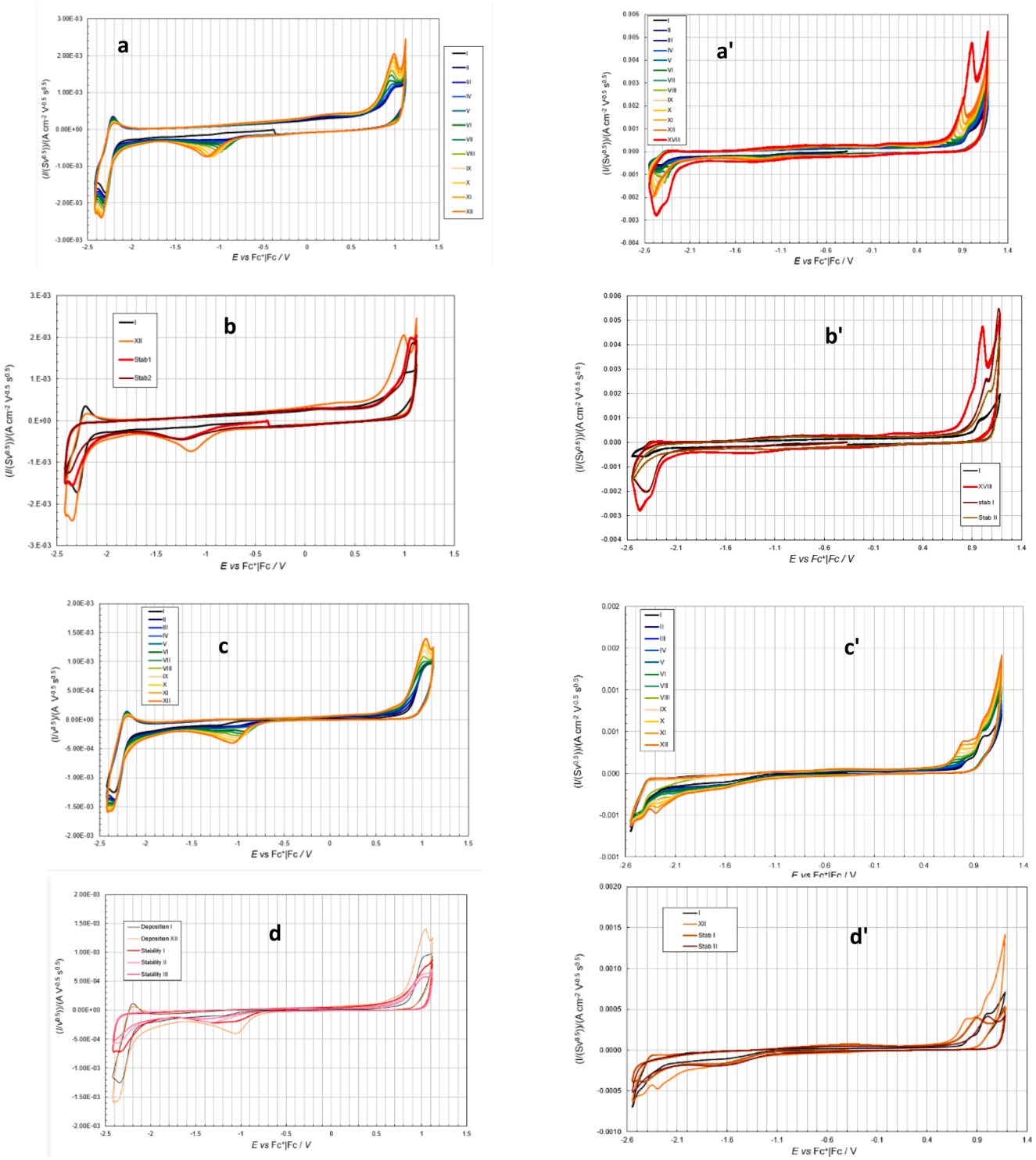

Fig. 5. Oxidative electrodeposition at 0.2 V/s potential scan rate of electroactive films from racemic dithiaaza[7]helicene **1** (left) and dithia[7]helicene **3** (right) in CH_3CN with 0.1 M $TBAPF_6$ supporting electrolyte. Selected electrodeposition cycles (a,a') and stability cycles (b,b') on GC electrodes; selected electrodeposition cycles (c,c') and stability cycles (d,d') on ITO electrodes.

nearly the same (0.30/0.31 eV).

The two azahelicenes **5** and **6** show a complex series of (quasi) reversible reduction peaks, with the same $E_{p,Ic} = -2.34$ V as well as a complex oxidation pattern starting with a first rather fast but chemically irreversible ET (Table 1, Fig. 4c, c', S16 and Fig. 4d, d', S17). Unfortunately, dealing with aza compounds in quite tiny amount, studying the oxidation onset signals was tricky and so far not resolutive, on account of the above mentioned aza peculiarities combined with the presence of low, irregular and hardly reproducible (pre?)peaks even after very careful sample purification, a feature that we plan to investigate in a further step. In any case, the 2-aza[7]helicene **5** features a less positive oxidation onset than aza[6]helicene **6**, which can be justified with the higher conjugation efficiency along the backbone and possibly also in 3D space.

To achieve clues on the localization of the redox sites it is useful to comparatively discuss the first reduction and first oxidation potentials of the five investigated helicenes (comparison graphically available in Figure S36). In particular, dithiaaza[7]helicene **1** has:

(i) its first reduction peak remarkably *less negative* than that of dithia[7]helicene **3** (by 0.14 V) and slightly *less negative* than those of azahelicenes **5** and **6** (by 0.04 V), too;
(ii) its first oxidation peak slightly *more positive* than that of dithia[7]helicene **3** (by 0.05 V) and (although close to the above tricky (pre?)peaks) significantly *less positive* than the first neat oxidation signal of azahelicenes **5** and **6** as well as of the two above discussed literature azahelicenes.

Such observations suggest that in the push-pull helicene **1** first reduction be mostly localized close to the isoquinoline terminal and first oxidation close to the BDT terminal.

Notably, the new molecule **1** appears to feature at the same time the easier reducibility of its azahelicene analogues and the easier oxidability of thiahelicenes, resulting in the smallest gap (3.27 eV) respect to its carba- (**S16/S17**), thia- (**3**), or aza- (**5/6**) analogues. Actually, **1** is even slightly more reducible than azahelicenes, possibly for the global more effective conjugation, while it is slightly less oxidable than thiahelicenes, maybe due to interactions between the BDT terminal with the electron-attracting nitrogen. This latter effect is not observed with the diarylethene precursor **2**, in which the terminals are not overlapping.

2.4. Electrodeposition of electroactive inherently chiral films

Another key difference between the investigated helicenes concerns the outcome of the first oxidation process. Upon potential cycling around the first oxidation potential, dealing with azahelicenes **5** or **6** only slight traces of electroactive products (not growing with increasing cycle number) could be observed on the electrode surface (Figures S32, S33).

Instead, quite differently, dealing with either racemic dithia[7]

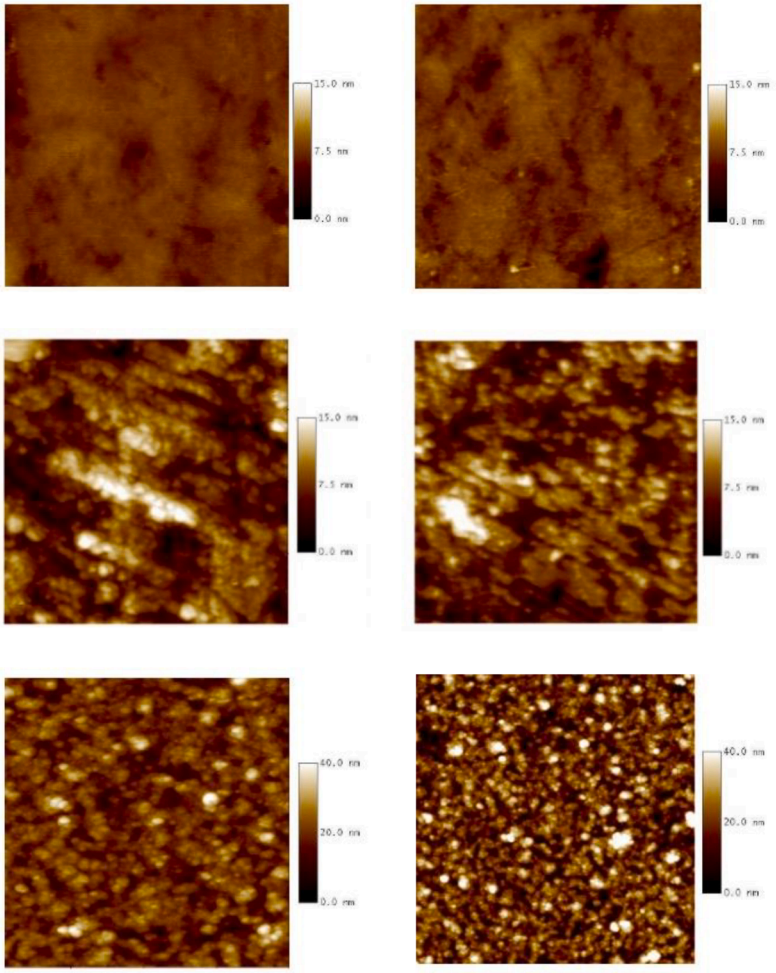

Fig. 6. Atomic Force Microscopy topography images collected on two different scan areas (1 × 1 μm^2, left; 2 × 2 μm^2 right) of ITO electrodes bare (top) and filmed with oligomer layers electrodeposited from dithiaaza[7]-helicene **1** (middle) or dithia[7]helicene **3** (bottom) with twelve oxidative potential cycles in CH_3CN with 0.1 M $TBAPF_6$ supporting electrolyte.

helicene **3** or racemic dithiaaza[7]helicene **1**, the electrodeposition of electroactive films was easily obtained (Figs. 5, S18-S23), similarly to the cited tetrathiahelicene electrooligomerization case [7]. Thus the presence of even a single BDT terminal enables the growth of an electroactive film (in this case very likely a dimer one), which was confirmed also in an experiment with open dithiaalkene precursor **4** (Figure S31). This also confirms that the first oxidation site in the dithiaaza[7]helicene involves the BDT terminal rather than N oxidation in the isoquinoline one.

Electrodeposition was successfully obtained on both GC and ITO, in CH_3CN and also, in some experiments in CH_2Cl_2 (protocol details in SI) in both cases with 0.1 M $TBAPF_6$ as supporting electrolyte. The film growth was very regular and reproducible in both cases **1** and **3**, but with remarkably different patterns (Figures S18-S23), pointing to a significant effect of the pyridine ring, when present (it must be however mentioned that in the case of **3** on ITO the peculiar cathodic CV pattern should involve a modification of the ITO surface [34]).

After deposition the films were submitted to a few more potential cycles in monomer free solution to check their stability and eliminate monomer traces for further investigation (SI). In this step they showed significant modifications upon cycling, appearing more labile than many former cases of thiophene-based oligomer films investigated in our laboratory, but stable enough for further characterizations.

Preliminary results of electrochemical impedance spectroscopy recorded on an electrodeposited oligo-**1** film at different potentials (Figure S34) look consistent with the corresponding charge states (negative/neutral/positive).

A first glimpse by Atomic Force Microscopy AFM at the morphology of films electrodeposited from the dithiaaza[7]helicene **1** or dithia[7]helicene **3** is provided in Fig. 6. Comparison with imaging of bare ITO surface confirms the filming of the electrode. In both cases globular particles with diameters of the order of a few tens of nm can be observed, with significant differences between films electrodeposited from helicene **1** and from helicene **3** in terms of both film texture and estimated root mean square (RMS) surface roughness (1.8 ± 0.4 nm for **1** vs 4.7 ± 1.0 nm for **3**). This points, again, to a significant role of the pyridine terminal in the film formation.

Extensive dedicated work will be of course required to achieve an all-around characterization of the films, which appears indeed worth of, considering the possibility to transfer and possibly amplify from monomer to electrodeposited film the peculiar combination of functional properties of helicene monomer **1** with the possible addition of powerful inherent chirality, starting from enantiopure monomers obtained by the above newly developed separation protocol.

3. Conclusions and perspectives

The new dithiaaza[7]helicene **1** designed, prepared and investigated by comparison with a pool of simpler heterohelicenes and related linear alkenes, thus providing further knowledge about helicene electrochemistry, appears an attracting electroactive molecular tool. It suggests us the image of a multipurpose Swiss knife with many potentialities, on account of

- its remarkable pool of functional scalar properties, even including complementary ones as a consequence of its featuring hetero-aromatic terminals of opposite character;
- its push-pull features with related peculiar electronic effects both along the backbone and even across space between the isoquinoline and the benzodithiophene terminal;
- its ability to easily and reproducibly electro-oligomerize into nano-structured electroactive films;
- its inherent chirality together with the availability of an effective newly developed enantioseparation protocol.

These features suggest many exciting developments. We look forward to more exhaustively investigating the scalar properties of the new molecular tool (especially on the isoquinoline side, including acid/base equilibria and possible alkylation to convert it into a molecular salt, since this first investigation was particularly focused on the benzodithiophene side) as well as the morphological and functional features of the (racemic) electrodeposited films.

Moreover, as a quantum leap in this research, we particularly look forward to preparing and characterizing inherently chiral films combining the above pool of functional properties with powerful chirality manifestations. The resulting outstanding materials could be tested in many contexts, starting from chiroptics (*e.g.* testing them for circularly polarized luminescence), spintronics (*e.g.* testing them in magnetoelectrochemistry experiments) and chiral electroanalysis (*e.g.* testing them in chiral voltammetry as inherently chiral electrode surfaces, besides testing their parent dithiaazahelicene as single molecule chiral additive in ionic liquid media).

CRediT authorship contribution statement

Luigi Menduti: Writing – review & editing, Investigation. **Stefano Magni:** Investigation. **Clara Baldoli:** Writing – review & editing, Investigation. **Silvia Rosa Araneo:** Writing – review & editing, Investigation. **Simona Rizzo:** Investigation. **Benedetta Bertolotti:** Investigation. **Alberto Bossi:** Writing – review & editing, Investigation, Conceptualization. **Marta Penconi:** Writing – review & editing, Investigation. **Francesco Orsini:** Writing – review & editing, Investigation. **Francesca Romana Mammone:** Investigation. **Claudio Villani:** Investigation. **Francesca Fontana:** Writing – review & editing, Supervision, Conceptualization. **Emanuela Licandro:** Writing – review & editing, Supervision, Conceptualization. **Patrizia Romana Mussini:** Writing – original draft, Supervision, Investigation, Conceptualization.

Declaration of competing interest

The authors declare that they have no known competing financial interests or personal relationships that could have appeared to influence the work reported in this paper.

Acknowledgements

The support of Università degli Studi di Milano for UNIMI-PSR (Piano di Supporto alla Ricerca) and availability of SmartMatLab advanced instrumentation is gratefully acknowledged. We are grateful to Dr. Roberto Cirilli (Istituto Superiore di Sanità, Roma) for his support and precious discussion concerning the chiral HPLC experiments on 2-aza[7]helicene. We also thank Chiara Margolfo (UNIMI) for useful discussion concerning ITO behaviour at negative potentials.

Supplementary materials

Supplementary material associated with this article can be found, in the online version, at doi:10.1016/j.electacta.2025.146188.

Data availability

Data will be made available on request.

References

[1] M. Gingras, One hundred years of helicene chemistry. Part 1: non-stereoselective syntheses of carbohelicenes, Chem. Soc. Rev. 42 (2013) 968, https://doi.org/10.1039/C2CS35154D.
[2] C.-F. Chen, Y. Shen, Helicene chemistry, from synthesis to applications, Springer, Berlin/Heidelberg, Germany, 2017, https://doi.org/10.1007/978-3-662-53168-6.
[3] Y. Shen, C.-F. Chen, Helicenes: synthesis and applications, Chem. Rev. 112 (2012) 1463, https://doi.org/10.1021/cr200087r.

[4] M. Rickhaus, M. Mayor, M. Jurlček, Strain-induced helical chirality in polyaromatic systems, Chem. Soc. Rev. 45 (2016) 154, https://doi.org/10.1039/C5CS00620.
[5] M. Gingras, One hundred years of helicene chemistry. Part 2: stereoselective syntheses and chiral separations of carbohelicenes, Chem. Soc. Rev. 42 (2013) 1007, https://doi.org/10.1039/C2CS35111K.
[6] Y.-H. Tian, G. Park, M. Kertesz, Electronic structure of helicenes, C2S helicenes, and thiaheterohelicenes, Chem. Mater. 20 (2008) 3266, https://doi.org/10.1021/cm702813s.
[7] S. Arnaboldi, S. Cauteruccio, S. Grecchi, T. Benincori, M. Marcaccio, A. Orbelli Biroli, G. Longhi, E. Licandro, P.R. Mussini, Thiahelicene-based inherently chiral films for enantioselective electroanalysis, Chem. Sci. 10 (2019) 1539, https://doi.org/10.1039/C8SC03337D.
[8] A. Bossi, L. Falciola, C. Graiff, S. Maiorana, C. Rigamonti, A. Tiripicchio, E. Licandro, P.R. Mussini, Electrochemical activity of thiahelicenes: structure effects and electrooligomerization ability, Electrochim. Acta 54 (2009) 5083, https://doi.org/10.1016/j.electacta.2009.02.026.
[9] J. Vacek, J. Hrbáč, T. Strašák, T. Církva, J. Sýkora, L. Fekete, J. Pokorný, J. Bulíř, M. Hromadová, J. Crassous, J. Storch, Anodic deposition of enantiopure hexahelicene layers, ChemElectroChem 5 (2018) 2080, https://doi.org/10.1002/celc.201800565.
[10] J. Hrbáč, V. Pavelka, J. Zadny, J. Crassous, L. Fekete, J. Pokorny, P. Vanyseke, J. Storch, J. Vacek, Redox and optically active carbohelicene layers prepared by potentiodynamic polymerization, Electrochem. Commun. 113 (2020) 106689, https://doi.org/10.1016/j.elecom.2020.106689.
[11] M. Gingras, One hundred years of helicene chemistry. Part 3: applications and properties of carbohelicenes, Chem. Soc. Rev. 42 (2013) 1051, https://doi.org/10.1039/C2CS35111K.
[12] T. Mori, Chiroptical properties of symmetric double, triple and multiple helicenes, Chem. Rev. 121 (2021) 2373, https://doi.org/10.1021/acs.chemrev.0c01017.
[13] M. Cei, L. Di Bari, F. Zinna, Circularly polarized luminescence of helicenes: a data-informed insight, Chirality 35 (2023) 192, https://doi.org/10.1002/chir.23535.
[14] F. Tani, M. Narita, T. Murafuji, Helicene radicals: molecules bearing a combination of helical chirality and unpaired electron spin, ChemPlusChem 85 (2020) 2093, https://doi.org/10.1002/cplu.202000452.
[15] P.V. Möllers, B. Göhler, H. Zacharias, Chirality induced spin selectivity-the photoelectron view, Isr. J. Chem. 62 (2022) e202200062, https://doi.org/10.1002/ijch.202200062.
[16] P.R. Mussini, S. Arnaboldi, M. Magni, S. Grecchi, G. Longhi, T. Benincori, Enantiomer discrimination in absorption spectroscopy and in voltammetry: highlighting fascinating similarities and connections, Curr. Opin. Electrochem. 37 (2023) 101128, https://doi.org/10.1016/j.coelec.2022.101128.
[17] K. Dhbaibi, L. Favereau, J. Crassous, Enantioenriched helicenes and helicenoids containing main-group elements (B, Si, N, P), Chem. Rev. 119 (2019) 8846, https://doi.org/10.1021/acs.chemrev.9b00033.
[18] F. Fontana, G. Carminati, B. Bertolotti, P.R. Mussini, S. Arnaboldi, S. Grecchi, R. Cirilli, L. Micheli, S. Rizzo, Helicity: a non-conventional stereogenic element for designing inherently chiral ionic Liquids for electrochemical enantiodifferentiation, Molecules 26 (2021) 311, https://doi.org/10.3390/molecules26020311.
[19] F. Fontana, B. Bertolotti, S. Grecchi, P.R. Mussini, L. Micheli, R. Cirilli, M. Tommasini, S. Rizzo, 2,12-Diaza[6]helicene: an efficient non-conventional stereogenic scaffold for enantioselective electrochemical interphases, Chemosensors 9 (2021) 216, https://doi.org/10.3390/chemosensors9080216.
[20] L. Menduti, C. Baldoli, S. Manetto, M. Bolte, H.-W. Lerner, G. Longhi, C. Villani, E. Licandro, M. Wagner, $(BO)_2$-doped tetrathia[7]helicene: a configurationally stable blue emitter, Angew. Chem. Int. Ed. 62 (2023) e202215468, https://doi.org/10.1002/ange.202215468.
[21] L. Menduti, C. Baldoli, S. Manetto, C. Villani, M. Penconi, S. Grecchi, S. Arnaboldi, G. Mazzeo, G. Longhi, M. Bolte, A. Virovets, H.-W. Lerner, M. Wagner, E. Licandro, $(BO)_2$-doped tetrathia[7]helicenes: synthesis and property-change induced by "BO bond inversion, Org. Chem. Front. (2025), https://doi.org/10.1039/D4QO01897D.
[22] J. Rocker, J.A. Dresel, L.A. Krieger, P. Eckhardt, A.M. Ortuño, W.R. Kitzmann, G. H. Clever, K. Heinze, T. Opatz Substitution effects on the photophysical and photoredox properties of tetraaza[7]helicenes, Chem. Eur. J. 29 (2023) e202301244, https://doi.org/10.1002/chem.202301244.
[23] M. Napagoda, L. Rulíšek, A. Jančařík, J. Klívar, M. Šámal, I.G. Stará, I. Starý, V. Šolínová, V. Kašiča, A. Svatoš, Azahelicene superbases as MAILD matrices for acidic analytes, ChemPlusChem 78 (2013) 937, https://doi.org/10.1002/cplu.201300258.
[24] S. Cauteruccio, A. Dreuw, P.R. Mussini, E. Licandro, Tetrathia-helicenes: an infinite source of inspiration, chapter 6, in: J. Crassous, I.G. Stará, I. Starý (Eds.), Helicenes; Synthesis, Properties and Applications, Wiley, 2022, https://doi.org/10.1002/9783527829415.ch6.
[25] H. Osuga, H. Suzuki, K. Tanaka, Practical synthesis of optically pure bifunctionalized heterohelicenes, Bull. Chem. Soc. Jpn. 70 (1997) 891, https://doi.org/10.1002/9783527829415.ch1.
[26] K.B. Jørgensen, Improved methodology for photocyclization reactions, Molecules 15 (2010) 4334, https://doi.org/10.3390/molecules15064334.
[27] F.B. Mallory, C.W. Mallory, in: W.G. Dauben (Ed.), Org. React. 30 (1984) 1–456. ISBN: 978-0-471-89013-3.
[28] J. Míše, F. Teplý, I.G. Stará, M. Tichý, D. Šaman, I. Císařova, P. Vojtíšek, I. Starý, A straightforward route to helically chiral N-heteroaromatic compounds: practical synthesis of racemic 1,14-Diaza[5]helicene and optically pure 1- and 2-Aza[6]helicenes, Angew. Chem. Intern. Ed. 47 (2008) 3188, https://doi.org/10.1002/anie.200705463.
[29] A. Bossi, P.R. Mussini, G. Farinola, M. Penconi, S. Cauteruccio, M.E. Thompson, E. Licandro, Sparkling organic phosphorescence from fluorinated tetrathia[7]helicenes: synthesis and photophysical, electrochemical and computational studies, Chem. Eur. J. 29 (2023) e202300339, https://doi.org/10.1002/chem.202300339.
[30] G. Gritzner, J. Kuta, Recommendations on reporting electrode potentials in nonaqueous solvents (Recommendations 1983), Pure Appl. Chem. 56 (1984) 461, https://doi.org/10.1351/pac198456040461.
[31] K. Meerholz, J. Heinze, Electrochemical solution and solid-state investigations on conjugated oligomers and polymers of the α-thiophene and the p-phenylene series, Electrochim. Acta 41 (1996) 1839, https://doi.org/10.1016/0013-4686(95)00503-X.
[32] C. Kim, T.J. Marks, A. Facchetti, M. Schiavo, A. Bossi, S. Maiorana, E. Licandro, F. Todescato, S. Toffanin, M. Muccini, C. Graiff, A. Tiripicchio, Synthesis, characterization, and transistor response of tetrathia-[7]-helicene precursors and derivatives, Org. Electron. 19 (2009) 1511, https://doi.org/10.1016/j.orgel.2009.08.018.
[33] C. Hansch, A. Leo, R.W. Taft, A survey of Hammett substituent constants and resonance and field parameters, Chem. Rev. 81 (1991) 165, https://doi.org/10.1021/cr00002a004.
[34] S. Bouden, A. Dahi, F. Hauquier, H. Randriamahazakam J. Ghilane, Multifunctional indium tin oxide electrode generated by unusual surface modification, Sci. Rep. 6 (2016) 36708, https://doi.org/10.1038/srep36708.